# Resonant metalenses for flexural waves in plates

Andrea Colombi[a)]

Department of Mathematics

Imperial College

South Kensington, London

SW7 2AZ, UK

a) e-mail: andree.colombi@gmail.com

## Abstract

The dispersion curves of a cluster of closely spaced rods supported by a thin plate are characterised by subwavelength bandgaps and slow group velocities induced by local resonance effects. A recent analytical study, Williams et al. [2015], has shown how the slow velocity branch depends, amongst other parameters, on the height of the rods that make up the cluster. Such metamaterial, offering easy-to-tune spatial velocity gradients, is a perfect candidate for building gradient index lenses such as Luneburg, Maxwell and 90° rotating Eaton. Here theoretical results are combined with numerical simulations to design and test metalenses for flexural waves. The lenses are obtained by tuning the height of the cluster of rods such that they provide the required refractive index profile. Snapshots and videos from three-dimensional numerical simulations in a narrow band centered at $\sim 4$ kHz are used to analyse the performances of three types of gradient index metalens (Luneburg, Maxwell and 90° rotating). **PACS numbers:** 43.40Dx,43.40At,43.40Fz,43.20Tb.


## I. Introduction

Gradient index (GRIN) lenses or flat-lenses have been known since Maxwell's early works for their capacity to bend and focus waves with less distortion and losses than classic lenses [Maxwell, 1853; Rudolf Karl Luneburg, 1964]. Compared to classic lenses, GRIN lenses modify the ray trajectories in the most natural way, i.e. using a smooth refractive index transition throughout the lens [Sarbort and Tyc, 2012]. If, on one hand this makes the lens free of aberrations and losses, on the other it requires ad-hoc composite structures that are very complicated to create. This obstacle was overcome, at the end of the last century, with the advent of photonic crystals [Yablonovitch, 1987] and metamaterials [Pendry et al., 1999] that popularised composite objects made of micro-structured and tunable media. Henceforth, GRIN devices based on metamaterials have been used as a showcase for transformation optics [Pendry et al., 2006; Leonhardt, 2006b] and (surface) plasmonics [Pendry et al., 2004], producing spectacular examples of the control of waves including, the much debated, features of wave cloaking and invisibility [Kundtz and Smith, 2010; Kadic et al., 2012; Leonhardt, 2006a; Fleury and Alù, 2014]. While applications initially remained limited to the realm of electromagnetic waves, recently, an increasing number of works have demonstrated that this new paradigm of wave control via metamaterials can be applied to mechanical waves (hence governed by Navier's equation) at very different length scales [Kadic et al., 2013; Wegener, 2013]. Examples of this duality between electromagnetic and elastic waves are the locally resonant acoustic metamaterial [Liu et al., 2000] made of soda cans fabricated by Lemoult et al. [2012] or, for flexural waves, the cluster of rods attached to a plate [Rupin et al., 2014; Achaoui et al., 2013]. Said metamaterial, made of rods attached to a plate with its potential broad applicability from ultrasonics to geophysics, is considered herein. Local resonances between the rods and the supporting plate create exotic dispersion curves for this metamaterial that, besides bandgaps, feature strong frequency dependent velocity contrasts at a very subwavelength scale; this is due to the hybridisation between the longitudinal resonances of the rods and the vertically polarised motion of the $A_0$ mode in the plate. Recently, Williams et al. [2015] have derived the analytical relationship for the dispersion curves of this medium, that among other parameters, depends on the rod height. Hence, a GRIN metamaterial can be obtained by spatially tuning the height of each rod that compose the cluster of resonators. Before William's analytical work was published, and with the goal of building a directional cloak, Colombi et al. [2015] studied circular arrangements of rods with a radially graded profile that can reduce the back scattering produced by an obstacle. Now, using a similar circular arrangement of rods and with the analytical dispersion relationship available, we can directly compute the height profile for any given refractive index function and hence build a metalens for flexural waves.

Luneburg, Maxwell and 90° rotating Eaton type lens are fascinating examples of circular GRIN lenses. Mainly used in optics, radio and microwaves [Pfeiffer and Grbic, 2010; Xu et al., 2014; Falco et al., 2011], each lens is characterised by a refractive index profiles that shape ray trajectories in a distinctive way [Rudolf Karl Luneburg, 1964; Sarbort and Tyc, 2012]. The 90° rotating Eaton lens is certainly the most complex to realise because it is characterised by a maximum refractive index of $n = 5$, while Maxwell and Luneburg have approximately $n$ =1.5 and $n$ =1.3 respectively.

This is not the first work on GRIN lenses for flexural waves: other groups have proposed to tune the plate thickness or to use composite materials or phononic crystals to create the index gradient [Climente et al., 2014; Jin et al., 2015]. Our work is however the first that exploits the slow velocity branch of an elastic resonant metamaterial and utilises it to build a resonant metalens.

We have chosen time domain numerical simulations computed with a parallel spectral element solver [Peter et al., 2011] to test the performances of the lenses. The simulations aim at being as close as possible as an actual experiment in the laboratory (e.g. no absorbing boundaries) because the results contained in this report will be used for an experimental validation with a setting similar to that in Rupin et al. [2014].

We proceed by recalling the dispersion relationship obtained by Williams et al. [2015] and combining it with the refraction index formula for the 3 types of GRIN lenses. The resulting transcendental equation is then solved for the height profile of each lens. Finally snapshots and videos from numerical simulations illustrate the behaviour of the lenses with a source in the kHz range.

## II. Results

To introduce and use the dispersion relationship obtained by Williams et al. [2015], we recall the metamaterial configuration and some important paramaters used for the derivation. The one-dimensional array of resonators, rods of constant height $h$ and circular section attached to a flexible one-dimensional support transmitting flexural waves (identical to the $A_0$ mode in a thin plate), is shown in Fig 1a. In spite of the problem being one dimensional, information about the cross-sectional area are important for both rods and plate. The material used for the (numerical) model is aluminium with density $\rho = 2710\ kg/m^3$ and Young's modulus $E = 69$ GPa. The rods are characterised by a diameter $d = 0.003$ m and a height $h$, while the one-dimensional supporting plate has a thickness $b = 0.006$ m and a depth $d$ equals to the spacing between rods $l = 0.015$ m. The metamaterial's dispersion, in the frequency $\omega$ and wavenumber $k$ space, can be accurately modelled using the longitudinal resonances of the rod, neglecting its flexural motion that plays a minor role [Rupin et al., 2014; Williams et al., 2015]. Before moving to the metamaterial's dispersion equation, we recall the dispersion relationship of the flexural waves in the one-dimensional support (equal to the $A_0$ mode in a plate), that is:

$$k = \sqrt[4]{\frac{\rho A_p \omega^2}{E I_p}}, \tag{1}$$

where $A_p$ represents the cross sectional area of the segment, and $I_p$ its inertia moment (Fig. 1a). After defining the mass of the rod and the segment over the unit cell (Fig. 1a) as $M_r$ and $M_p$ respectively, we write the dispersion equation as [Eq. 32 in Williams et al., 2015]:

$$k_{eff} = \sqrt[4]{k\left(\frac{M_r}{M_p}\frac{\tan(kh)}{kh}\right) + 1}. \tag{2}$$

As expected the hybrid mode induced by the local resonance between plate and rods, profoundly differs from the $A_0$ mode of the bare plate given by Eq. (1). The difference is highlighted in Fig. 1b where the dispersion for an array of rods of $h = 0.6$ m is compared to that of the bare plate. Besides two bandgaps at approximately 2 and 6 kHz, we notice two asymptotically flat branches occurring close to the longitudinal modes of the rod, this is the hallmark of slow group velocities. The frequency dependent velocity profile, used later as input to design the GRIN lens, is easily derived from Eq. (2) through the relationship $k = \omega/v_p$:

$$v_{eff} = \left[ v_p \left( \frac{M_r}{M_p} \frac{\tan(kh)}{kh} \right) + 1 \right]^{-1/4}, \tag{3}$$

where $v_p$ represents the $A_0$ mode wavespeed derived from Eq. (1). As previously anticipated, in Fig. 1c, as we get close to the bandgaps the velocity approaches zero. A second striking feature of this plot is that the effective velocity in the metamaterial and in the plate overlaps only at one discrete frequency ($\sim 4.2$ kHz in this case). Hence, if we consider an incoming wave, the abrupt velocity change from plate to metamaterial will produce a diffraction pattern at all frequencies except at the crossing point. This phenomenon is likely to be at the root of the directional cloak studied by Colombi et al. [2015] when the analytical dispersion formula was not yet available. Therefore, to limit the reflection caused by diffraction between metamaterial and plate in the numerical results, we work between 4 and 4.4 kHz, around the equal effective velocity point (Fig. 1c). The strategy used to build the metalens is outlined in Fig. 1d. At any frequency located before

| Lens type | $n(r)$ |
|---|---|
| Luneburg | $\sqrt{2-\frac{r^2}{R^2}}$ |
| Maxwell | $2/(1+\frac{r^2}{R^2})$ |
| 90° | $rn^4-2n+r=0$ |

Table 1: Refractive index for each lens as a function of the radial coordinate $r$.

the bandgap, say, here at 4 kHz, the group velocity is inversely proportional to the rod's height. The curve at 4.4 kHz exhibits a kink at lower speed because it is located on to the bandgap when the height of the rod is increased. The significant velocity drop allows us to design GRIN lenses with very strong refractive index variation such as the Luneburg, Maxwell and 90° rotating Eaton type developed in this study. All are characterised by a circular shape with radius $R$ =0.18 cm while the refractive index for each lens is given in Tab. 1 as a function of the radial coordinate $r$. The refraction index $n$ between two media, say, material 0 and material 1 can be formulated in terms of the ratio of velocity contrast $n=\dfrac{v_0}{v_1}$. We combine this latter definition with the lens refractive index profiles (Tab. 1) and we plug it into Eq. (3) to obtain a relationship that relates the rod's height profile to refractive index. The result is the following transcendental equation where the right-hand-side depends on the refractive index profile $n(r)$ (Tab. 1):

$$\frac{\tan(kh)}{kh} = \frac{M_p}{M_r}\left[\left(n(r)\frac{v_p}{v_0}\right)^4 - 1\right]. \tag{4}$$

Here $v_p$ is the $A_0$ mode wavespeed obtained from Eq. (1) through $k = \omega/v_p$ and $v_0$ is the input wavespeed at $r = R$. Since at $r = R$ the rods have $h = 0.6$ m and at 4 kHz $v_p = v_0$ the transition from plate to metamaterial takes place smoothly. The root of Eq. (4) over the interval $k = [0, \pi]$ represents the rod's height that provides the sought refractive index. Contrary to the original derivation of the dispersion curves in Williams et al. [2015], where the metamaterial was infinite, and with constant rod's height, the metalenses have radially varying profile over a finite area as shown in Fig. 2. The very positive results presented in this letter indicate that Williams et al. [2015] approach remains robust although not all fundamental assumptions are met precisely; the height and effective velocity profile for each metalens are gathered together in Figs. 1b-d. Notice that for the 90° case, the velocity is truncated at 100 m/s to avoid working too close to the bandgap where $v_{eff}$ is zero; this approximation has little to no effect on the lens behaviour. We notice that the height profiles in Fig. 2 are negatively correlated with the plate thickness profile obtained in other implementations of the GRIN lens by Lefebvre et al. [2015] and Climente et al. [2014]. In the cited studies the plate thickness is decreasing, while here the height of the rods is increasing towards the center. The anti-correlation can be explained considering the following expression for the refractive index $n$ in a thin plate of thickness $b$:

$$n = \frac{1}{v_{eff}} = \sqrt[4]{\frac{12\rho(1-\nu^2)}{Eb^2\omega^2}}, \tag{5}$$

where $\nu$ is the Poisson's ratio of the material. To achieve high value of $n$ (hence low $v_{eff}$), $b$ must decrease toward the center of the lens. In this study, we do not act on $b$ but, through the resonance of the rod, on the effective density $\rho$ appearing at the numerator and hence anti-correlated .

The performance of these metalenses is verified using the well tested numerical code SPECFEM3D [Peter et al., 2011], a spectral element solver for time domain elastodynamics. Details concerning the model discretisation and implementation of the simulations can be found in previous publications [Colombi et al., 2014, 2015]. The model consists of a 6 mm-thick plate whose shape and dimension are given in Fig. 2 supporting the cluster of resonators. Both are made of aluminium. The metalens is positioned approximatively at the center of the plate and the boundaries are all traction-free as in an actual laboratory set-up. Rods, are regularly distributed with a 15 mm spacing. This spacing guarantees the metamaterial to be very subwavelength at this frequency ($\lambda$, the wavelength, varies between 15 to 7 cm in the 1-10 kHz band). While the regular spacing was chosen to ease the meshing of the model, in practice periodicity is not required since the metamaterial is very subwavelength and hence resilient to disorder. Depending on the type of lens, the source generating flexural waves is implemented differently. For the

Luneburg type we have used a plane wave, for the Maxwell type a point force located on one side of the lens while for the Eaton type we used a Gaussian beam like source. Regardless of the source shape, they are all driven in time by a broadband Ricker pulse [Komatitsch and Tromp, 1999]. The wavefield in the plate is then filtered between 4 and 4.4 kHz. Snapshots of the wavefield are shown in Fig. 3 for the different types of lenses. The videos associated with these simulations are available as supplementary material. We notice that, despite the reverberations produced by plate borders, the lensing effect is clearly visible. The results suggest that a laboratory experiment with a set up similar to that of Rupin et al. [2014] would be perfectly feasible. Although not visible in the snapshots the initial transient regime of the metamaterial is clearly visible in the videos: In the first instance part of the energy is taken by the resonators and only after a fraction of a millisecond the system reaches a more stationary condition. This transient behaviour can be seen as the time taken by the energy to be equipartitioned between the rods and the plate in the metamaterial. This timelag is comparable to the resonance period of the rod approximately 0.15 ms for the longitudinal mode at ∼6 kHz.

**Mm. 1.** Video Luneburg lens.

**Mm. 2.** Video Maxwell lens.

**Mm. 3.** Video 90° Eaton rotating lens.

## III. Conclusion

We have tested numerically 3 types of GRIN lenses for flexural waves based on a recently developed locally resonant metamaterial. The metamaterial is made of a cluster of circularly arranged, closely spaced rods attached to a plate and shows strong velocity variations directly proportional to frequency and rod's height. This latter parameter has been used to obtain the required refractive index variation that characterises each lens. By using a laboratory model made of aluminium the lenses will be easily manufactured and tested in an actual laboratory experiment. Starting from the similarity between the case of the plate and a halfspace with resonators [Colombi et al., 2016], metalenses can be designed for Rayleigh waves.

## REFERENCES

Achaoui, Y., Laude, V., Benchabane, S., and Khelif, A. (2013). Local resonances in phononic crystals and in random arrangements of pillars on a surface. *J. Appl. Phys.*, 114(10):–.

Climente, A., Torrent, D., and Sánchez-Dehesa, J. (2014). Gradient index lenses for flexural waves based on thickness variations. *Appl. Phys. Lett.*, 105:064101.

Colombi, A., Roux, P., Guenneau, S., Gueguen, P., and Craster, R. (2016). Forests as a natural seismic metamaterial: Rayleigh wave bandgaps induced by local resonances. *Sci. Rep.*, 5(5):19238.

Colombi, A., Roux, P., Guenneau, S., and Rupin, M. (2015). Directional cloaking of flexural waves in a plate with a locally resonant metamaterial. *J. Acoust. Soc. Am.*, 137(4):1783–9.

Colombi, A., Roux, P., and Rupin, M. (2014). Sub-wavelength energy trapping of elastic waves in a meta-material. *J. Acoust. Soc. Am.*, 136(2):EL192–8.

Falco, A. D., Kehr, S. C., and Leonhardt, U. (2011). Luneburg lens in silicon photonics. *Opt. Express*, 19(6):5156–5162.

Fleury, R. and Alù, A. (2014). Cloaking and invisibility: A review. *Forum for Electromagnetic Research Methods and Application Technologies (FERMAT)*, page 23.

Jin, Y., Torrent, D., Pennec, Y., Pan, Y., and Djafari-Rouhani, B. (2015). Simultaneous control of the s0 and a0 lamb modes by graded phononic crystal plates. *Journal of Applied Physics*, 117(24):–.

Kadic, M., Buckmann, T., Schittny, T., and Wegener, M. (2013). Metamaterials beyond electromagnetism. *Report Progress Physics*, 76:126501.

Kadic, M., Guenneau, S., Enoch, S., Huidobro, P. A., Martín-Moreno, L., García-Vidal, F. J., Renger, J., and Quidant, R. (2012). Transformation plasmonics. *Nanophotonics*, 1:51–64.

Komatitsch, D. and Tromp, J. (1999). Introduction to the spectral element method for three-dimensional seismic wave propagation. *Geophysical Journal International*, 139(3):806–822.

Kundtz, N. and Smith, D. R. (2010). Extreme-angle broadband metamaterial lens. *Nat. Mater*, 9(2):129–132.

Lefebvre, G., Dubois, M., Beauvais, R., Achaoui, Y., Ing, R. K., Guenneau, S., and Sebbah, P. (2015). Experiments on maxwell's fish-eye dynamics in elastic plates. *Applied Physics Letters*, 106(2).

Lemoult, F., K., N., F., M., and Lerosey, G. (2012). Wave propagation control at the deep subwavelength scale in metamaterials. *Nature Physics*, (1):55–60.

Leonhardt, U. (2006a). Notes on conformal invisibility devices. *New J. Phys.*, 8:118.

Leonhardt, U. (2006b). Optical conformal mapping. *Science*, 312(5781):1777–1780.

Liu, Z., Zhang, X., Mao, Y., Zhu, Y. Y., Yang, Z., Chan, C. T., and Sheng, P. (2000). Locally resonant sonic materials. *Science*, 289(5485):1734–1736.

Maxwell, J. (1853). Problems. *The Cambridge and Dublin mathematical journal (Macmillan)*, 8:188.

Pendry, J., Holden, A. J., Robbins, D. J., and Stewart, W. J. (1999). Magnetism from conductors and enhanced nonlinear phenomena. *Microwave Theory and Techniques, IEEE Transactions on*, 47(11):2075–2084.

Pendry, J. B., Martin-Moreno, L., and Garcia-Vidal, F. (2004). Mimicking surface plasmons with structured surfaces. *Science*, 305:847–848.

Pendry, J. B., Schurig, D., and Smith, D. R. (2006). Controlling electromagnetic fields. *Science*, 312(5781):1780–1782.

Peter, D., Komatitsch, D., Luo, Y., Martin, R., Le Goff, N., Casarotti, E., Le Loher, P., Magnoni, F., Liu, Q., Blitz, C., Nissen-Meyer, T., Basini, P., and Tromp, J. (2011). Forward and adjoint simulations of seismic wave propagation on fully unstructured hexahedral meshes. *Geophys. J. Int.*, 186(2):721–739.

Pfeiffer, C. and Grbic, A. (2010). A printed, broadband luneburg lens antenna. *IEEE Transactions on Antennas and Propagation*, 58(9):3055–3059.

Rudolf Karl Luneburg, M. H. (1964). *Mathematical Theory of Optics*. University of California Press. 1st edition.

Rupin, M., Lemoult, F., Lerosey, G., and Roux, P. (2014). Experimental demonstration of ordered and disordered multi-resonant metamaterials for lamb waves. *Phys. Rev. Lett.*, 112:234301.

Sarbort, M. and Tyc, T. (2012). Spherical media and geodesic lenses in geometrical optics. *Journal of Optics*, 14(7):075705.

Wegener, M. (2013). Metamaterials beyond optics. *Science*, 342(6161):939–940.

Williams, E. G., Roux, P., Rupin, M., and Kuperman, W. A. (2015). Theory of multiresonant metamaterials for $A_0$ lamb waves. *Phys. Rev. B*, 91:104307.

Xu, H. X., Wang, G. M., Tao, Z., and Cai, T. (2014). An octave-bandwidth half maxwell fish-eye lens antenna using three-dimensional gradient-index fractal metamaterials. *IEEE Transactions on Antennas and Propagation*, 62(9):4823–4828.

Yablonovitch, E. (1987). Inhibited spontaneous emission in solid-state physics and electronics. *Phys. Rev. Lett.*, 58:2059–2062.

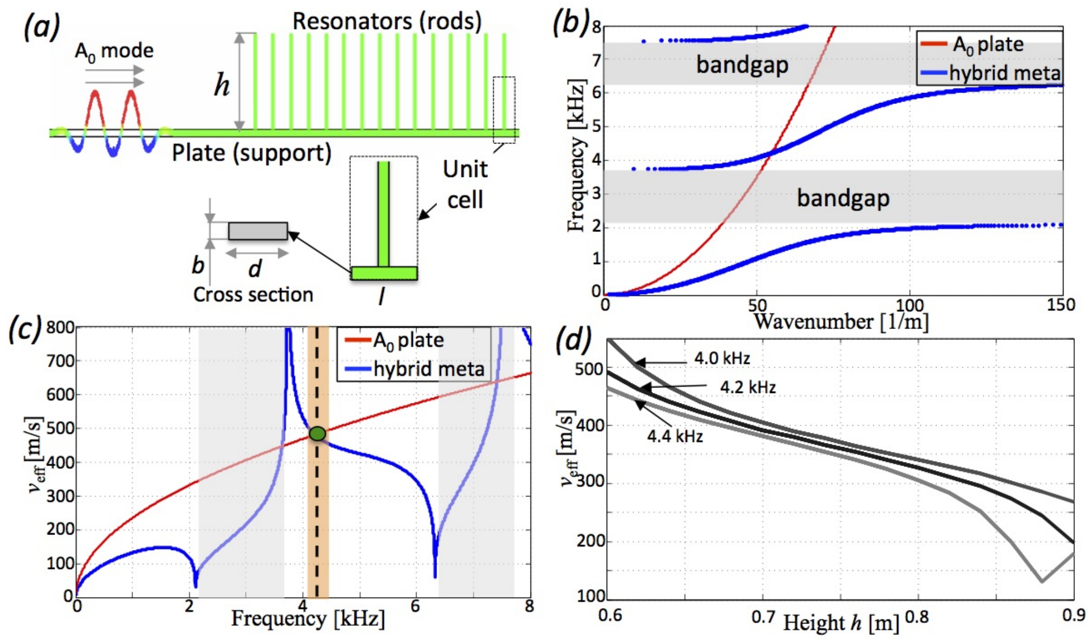


Figure 1: Dispersion properties of the metamaterial. (a) The set-up similar to that used in Williams et al. [2015] to the derived Eq. (2). (b) Dispersion curves for metamaterial and bare plate. (c) Effective velocity in the metamaterial and in the bare plate. The equal velocity frequency is highlighted. (d) Effective velocity in the metamaterial as a function of the rod's height for the frequency band used to test the metalenses. (Color online).

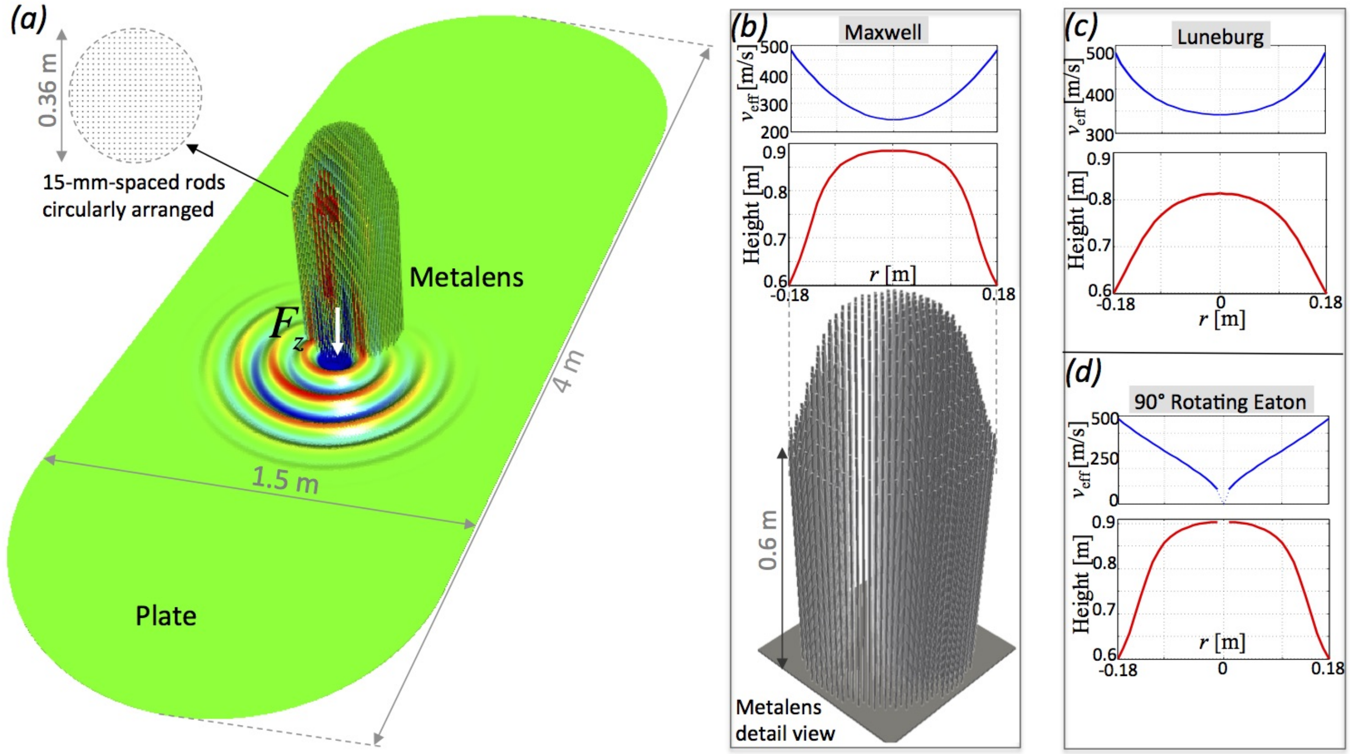


Figure 2: (a) Numerical model of the cluster of rods and the plate used in the simulations. (a-d) Different heights and effective velocity profiles for the three types of metalenses. (Color online).

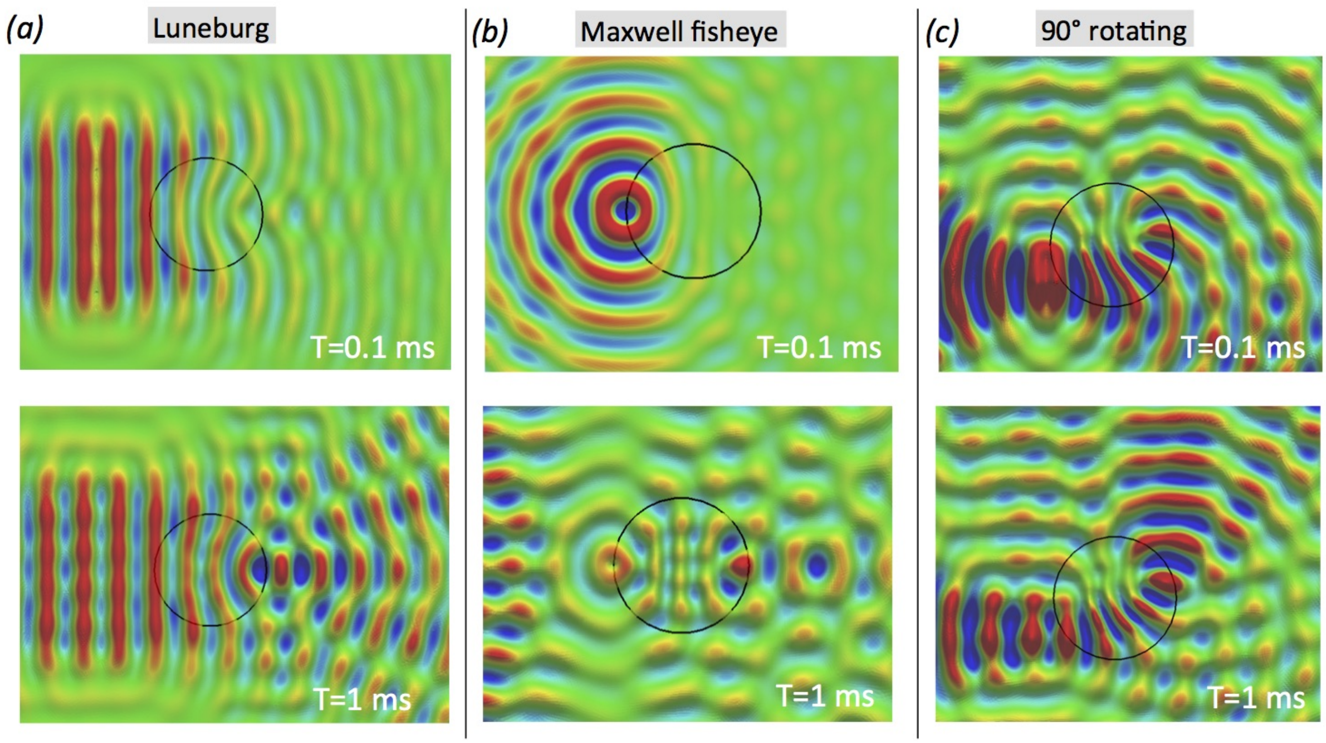


Figure 3: Snapshots at different time of the vertical component of the wavefild showing the behaviour of each metalens. The lens circular boundary is highlighted in black. Videos available as suplementary material. Wavefields are passband filtered between 4 and 4.4 kHz. The amplitude is normalised. (Color online).